Three-flavor instantaneous normal mode formalism: Diffusion, harmonicity, and the potential energy landscape of liquid CS_2

Wu-Xiong Li and T. Keyes[a)]
Department of Chemistry, Boston University, Boston, Massachusetts 02215

Francesco Sciortino
Dipartimento di Fisica and Istituto Nazionale per la Fisica della Materia, Universita di Roma La Sapienza, P.le Aldo Moro 2, I-00185, Roma, Italy

(Received 30 June 1997; accepted 24 September 1997)

Instantaneous normal modes are classified by their one-dimensional potential energy profiles, $U(q)$, into single well (SW), double well (DW), and shoulder potential (SH) modes. It is proposed that the resulting three-flavor description replace the current two-flavor division into real or imaginary frequency modes, and that the DW modes replace Im ω in theories of diffusion. Calculations of the three-flavor densities of states are presented for normal and supercooled liquid CS_2, and the self-diffusion constant, $D(T)$, is related to the DW modes. Indicators of strength/fragility are given based on the relative numbers of different mode types, and indicators of harmonicity are constructed by comparison of simulated instantaneous normal modes properties with the predictions of the harmonic approximation. It is found that the SW modes are harmonic in an intermediate Re ω range $20\ \mathrm{ps}^{-1} > \omega > 2.5\ \mathrm{ps}^{-1}$, and the anharmonicity at high and low ω is explained in terms of the potential energy ''landscape.'' DW modes are remarkably harmonic over the full range of Im ω. The T dependence of the diffusion constant is also interpreted in terms of the landscape, as manifested primarily in the properties of the energy barriers to diffusion. Diffusion is clearly associated with the strongly T-dependent crossing of barriers with $\omega \sim 3\ \mathrm{ps}^{-1}$. © *1998 American Institute of Physics.* [S0021-9606(98)50901-4]

I. INTRODUCTION

A new description[1–3] of liquid state dynamics is based upon instantaneous normal modes (INM). The INM are the eigenfunctions of the Hessian, the matrix of second derivatives of the potential energy, U, with respect to the mass-weighted atomic or molecular coordinates. The frequencies ω_α are the square roots of the eigenvalues, the density of states (dos) for a single configuration is $\rho(\omega) = \Sigma \delta(\omega - \omega_\alpha)$ and the averaged dos is $\langle \rho(\omega) \rangle$. In a liquid, some eigenvalues are negative, indicating downward curvature of the potential surface and yielding imaginary frequencies. Im ω are conventionally displayed as negative ω, and $\langle \rho(\omega) \rangle$ becomes a sum of two distinct lobes, $\langle \rho(\omega) \rangle = \langle \rho_s(\omega) \rangle + \langle \rho_u(\omega) \rangle$, with the ''stable'' ($s$) Re ω on the positive real ω axis and the unstable (u) Im ω on the negative. Reference to a positive ω for an Im ω mode indicates $|\omega|$. The terminology indicates that Re ω harmonic modes are stable oscillators [$\cos(\omega t)$], while Im ω modes exhibit unstable exponential growth ($\cosh \omega t$).

Separate treatment of the Re ω and Im ω modes leads to a two-flavor INM formalism. A simple idealization[3] is that the Re ω modes are finite-lifetime harmonic oscillations about the local minima of U, in the wells or basins, while the Im ω modes are representative of the tops of the barriers crossed in activated hopping of the system from basin to basin. Consequently INM fits very well with the idea[4] that the topology of the potential energy surface, or landscape, is crucial to the properties of liquids. Several theories[2,3,5–11] of time correlation functions have employed the Re ω modes, or, at short times, all the INM. The picture of interrupted harmonic oscillations is particularly well suited for systems of low fluidity, e.g., supercooled liquids. We have presented[3,12,13] theories of the averaged barrier crossing rate, ω_h, in terms of $\langle \rho_u(\omega) \rangle$. The lowest Im ω modes must be excluded in order to reproduce activated, exponential T dependence of the self-diffusion constant, $D(T)$. We proposed[3,12,13] that such modes might represent anharmonicities unrelated to barriers. Bembenek and Laird[14] calculated the one-dimensional potential energy profiles along the INM, $U(q)$, for Lennard-Jones (LJ) and smooth spheres and found Im ω profiles of two types, barrier crossing double wells (DW) and ''shoulder'' (SH) potentials, single wells with shoulders. They gave the DW dos, $\langle \rho_{\mathrm{DW}}(\omega) \rangle$, which indeed vanishes for $|\omega| < \omega_c$, where ω_c is a cutoff.

It has always been clear[3,7,12] that some ''false-barrier'' Im ω modes do not contribute to $D(T)$, since they persist while D vanishes at T_g. In Ref. 7, we simply subtracted the modes remaining at T_g. Use of the DW is more systematic, but hardly the last word. Vijayadamodar and Nitzan[15] introduced ''zero force'' modes, which exclude the SH and require that the system is very close to the barrier top. Bembenek and Laird[14] proposed that diffusion requires extended DW modes, meaning that the participation ratio exceeds a threshold value. Gezelter *et al.* have noted[16] that the configurations from both sides of the barrier for some DW in LJ can quench to the same local minima of the N-body U, suggesting another criterion for false barriers. On the other hand, in

a)Electronic mail: keyes@chem.bu.edu

 0021-9606/98/108(1)/252/9/$15.00

water, one of us and Tartaglia[9] recently found that the fraction, f_{DW} of DW modes [area of $\langle \rho_{\mathrm{DW}}(\omega) \rangle$] vs T extrapolates to zero at the ideal kinetic glass transition temperature,[17] T_c. Relative to molecular liquids, atomic liquids have much higher total fractions of Im ω modes, f_{Im}, of DW modes and of false-barrier DW modes. The DW are a good approximation to the barrier modes for water and we suggest, in general, for[18] strong liquids. In Angell's categorization,[18] atomic liquids are fragile and water is strong; we believe that a large fraction of DW modes is a signature of fragility. Water may not conventionally be considered strong, due to the observed weak T dependence of viscosity, but Angell[18] has argued that characteristic Arrhenius T dependence would be seen if experimental cooling rates were high enough to avoid crystallization and achieve sufficiently low T.

In molecular liquids, diffusion must be calculated[7] from *translational* barrier-crossing INM, given to first approximation by the translational DW modes. Translational and rotational dos, denoted tr and rot, have been constructed[2,5] by weighting the contribution of each mode by the translational or rotational projection of its eigenfunction. Recently,[19] we calculated a ''pure translation'' (TR) dos for CS_2 from the Hessian of derivatives with respect to the molecular center-of-mass coordinates, and found that the Im ω TR modes vanished at T_g, while[7] the tr do not. Thus, we believe that false-barrier modes in molecular liquids are primarily caused by rotation which is not removed by the projection method. The issue does not arise in water because hydrogen bonding suppresses the Im ω rot.

With the Im ω modes divided into DW and SH, the single well (SW) harmonic oscillations complete the picture, a three-flavor INM formalism. The SW all have Re ω and, except for very few SH modes, all Re ω modes are SW; SW and Re ω are essentially interchangeable. The first article to present this viewpoint in full is Ref. 9. The terminology employed therein, also used by Bembenek and Laird,[14] is stable and unstable for SW and DW, conflicting with our prior usage. Consistent use of Re, Im, SW, DW, and SH with no reference to stable and unstable is unambiguous, and that will now be our convention.

We report results on CS_2 at $P=1$ atm and T spanning the normal and supercooled liquid range, $298\ \mathrm{K} > T > 100\ \mathrm{K}$. The melting point is $T_m = 165$ K, and we estimate a glass transition $T_g \sim 100$ K. We will discuss general properties of the three-flavor dos and their relation to diffusion and to strength/fragility. Considerable information, such as the distribution of energy barrier heights, and the mean square displacement, $\langle q^2 \rangle$, along a normal coordinate may simply be read off from the $U(q)$. These data are of fundamental interest, reveal properties of the landscape, and are also required as components of INM-based theories, CS_2 lies between LJ and water on the strong/fragile scale, providing a test of our ideas about INM and strength/fragility.

The harmonicity of liquids may be probed by comparing harmonic expressions for INM properties with results from simulation. In Ref. 9, the ratio, $(\omega_{\mathrm{min}}/\omega_{\mathrm{inm}})^2$, was proposed as a measure of harmonicity of the SW/INM, where ω_{min} is the frequency at the bottom of the SW and ω_{inm} is the actual frequency. For a harmonic well, the ratio equals unity. In supercooled and normal liquid water, it is[9] equal to unity for $\omega > 40\ \mathrm{cm}^{-1}$, and rises sharply for lower ω. Thus one may say that the modes of water are harmonic for $\omega > 40\ \mathrm{cm}^{-1}$. We will investigate the harmonicity of CS_2 in similar fashion.

II. SIMULATION AND THREE-FLAVOR DENSITIES

Liquid CS_2 is simulated at $P=1$ atm, with the intermolecular potential of atom-atom LJ interactions given by[20] Tildesley and Madden. Harmonic bond stretch and bend potentials plus[21] a harmonic coupling of the two stretches are also included. The intramolecular force constants are adjusted to obtain the correct bend, symmetric stretch, and antisymmetric stretch frequencies of an isolated molecule. Although the model includes molecular vibration, the subjects of this article are the intermolecular INM. The molecular dynamics algorithm is our synthesis[12] of the multiple time step method[22] and the Hoover–Evans constant kinetic energy scheme[23] applied to center-of-mass motion at constant volume. The intermolecular time step is 0.75 fs with 10 short steps/intermolecular step for the intramolecular forces. Constant center-of-mass kinetic energy approximates constant T and avoids temperature echoes during quenches. For each temperature, the correct density is used, with supercooled densities obtained[7] by extrapolation from the normal liquid. With basic time and distance units as picoseconds and angstrom, we choose[7] a mass unit, denoted μ, such that energy comes out in degrees Kelvin; $\mu = 0.8315$ amu.

A hot ($T=600$ K) liquid is equilibrated for 75 ps at the desired density, quenched to the T of interest in one step, and first equilibrated for 5.2 ps while the intramolecular temperature is forced to equal the intermolecular T every long time step. Having achieved intermolecular-intramolecular equilibrium, the system is equilibrated normally for 30 ps. At least 200 configurations were sampled in the data gathering period, saved every 1.5 ps. The time-dependent potential energy and pair distribution function are monitored for evidence of solidification. CS_2 is encouragingly resistant to solidification but some runs show a slight downward drift of the potential energy and we discard them. Standard numerical eigenanalysis is applied to the Hessian, and for each mode, we obtain $U(q)$. Starting at a configuration R_0, U is evaluated at 1100 configurations in both directions along the mode; q points are spaced by $0.024\ \sqrt{\mu}$Å. The profile is first checked for the number of minima; with two it is a DW, with one SW or SH. The single-minimum modes are separated by the behavior of $U''(q)$, which has no zeros for a SW and vice-versa. Typical $U(q)$ at 165 K are in Fig. 1.

The three dos at the normal melting point, 165 K, are displayed in Fig. 2. On the Im ω side, a DW cutoff is visible and the SH modes dominate at low ω, the DW at high ω. To a good approximation, all of the Re ω INM are SW, but a tiny SH lobe exists. Figures 3 and 4 show the SW and DW densities at $T_g = 100$, $T_m = 165$, 224, and 298 K. Away from the lowest ω, the SW dos equals the Re ω dos; we charac-

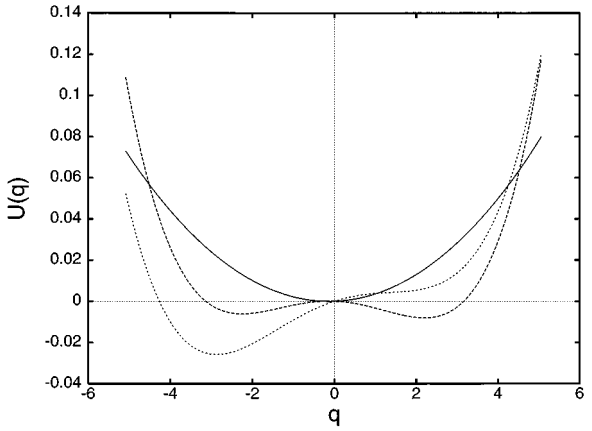

FIG. 1. Representative SW (solid line), DW (large dash), and SH potential energy profiles $U(q)$; U in $N*T$, N number molecules (108), T temperature in K (165 K).

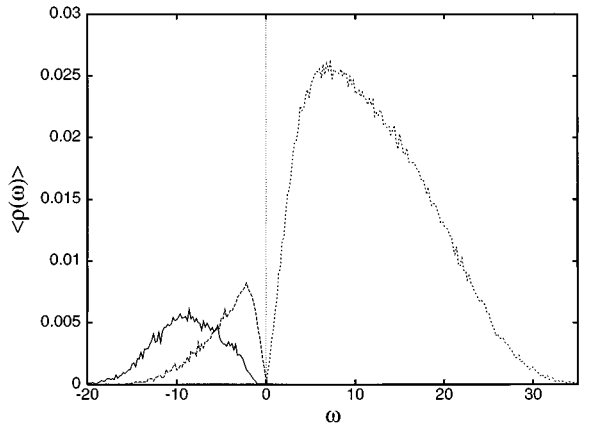

FIG. 2. SW (positive ω), DW (solid), and SH densities at 165 K; ω in ps^{-1}.

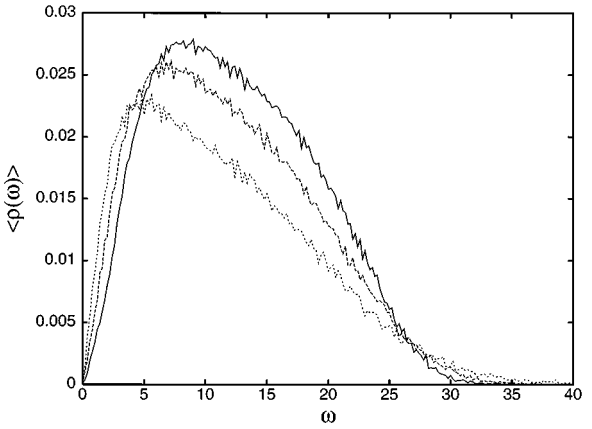

FIG. 3. SW density at 100 (solid), 165 (large dash), and 298 K; ω in ps^{-1}.

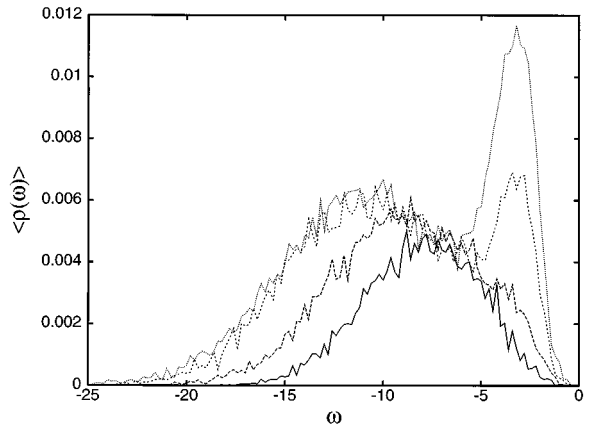

FIG. 4. DW density at 100 (solid), 165 (large dash), 244 (small dash), and 298 K; ω in ps^{-1}.

terized the latter in Ref. 7. With increasing T, the peak shifts to lower ω due to the decrease in density at constant P, while the high-ω wing extends due to more hard, close molecular interactions. These effects combine to create an isobestic point at $\omega \sim 27\ \mathrm{ps}^{-1}$, with $\langle \rho_{\mathrm{SW}}(\omega) \rangle$ increasing with increasing T for $\omega > 27\ \mathrm{ps}^{-1}$ and vice-versa for intermediate ω.

The DW (Fig. 4) clearly show the cutoff ω_c which increases with decreasing T, varying from $\sim 0.4\ \mathrm{ps}^{-1}$ at $T = 298$ K to $\sim 1.2\ \mathrm{ps}^{-1}$ at $T = 100$ K. In Ref. 7, the IM ω lobe was seen to consist of a strongly T-dependent translational low-ω spike, which governs diffusion, sitting upon a weakly T-dependent broad rotational background. The DW dos also shows this structure, with the translational spike at $|\omega| \sim 3.2\ \mathrm{ps}^{-1}$ exhibiting strong T dependence for $T > T_m$. Figure 5 is a blowup of the low-ω region at 298 K. The Re ω and Im ω densities are linear in $|\omega|$ at low ω, in contrast to the Debye ω^2 behavior. Despite the small amplitude of the SH dos, removing it from the Re ω dos yields a SW dos with some curvature at low ω, and the DW dos is not at all linear. The highest Re ω at which a SH can be found is roughly equal to ω_c, a symmetry which we have proposed[24] elsewhere. All the dos are identically zero at $\omega = 0$, and the ap-

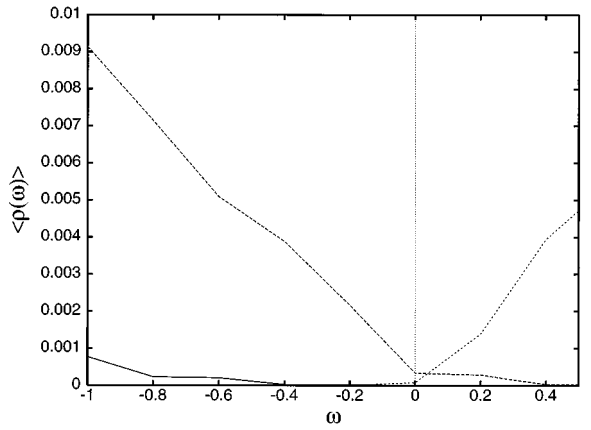

FIG. 5. Blow up of low Re ω region at 298 K showing DW with cutoff (solid), SH with small Re ω lobe (large dash), and SW.

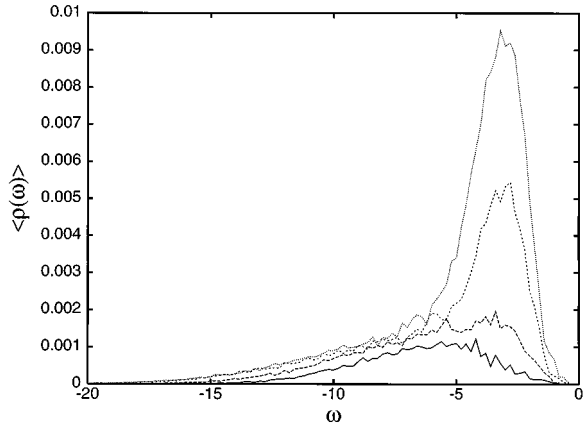

FIG. 6. As Fig. 4 for translational DW.

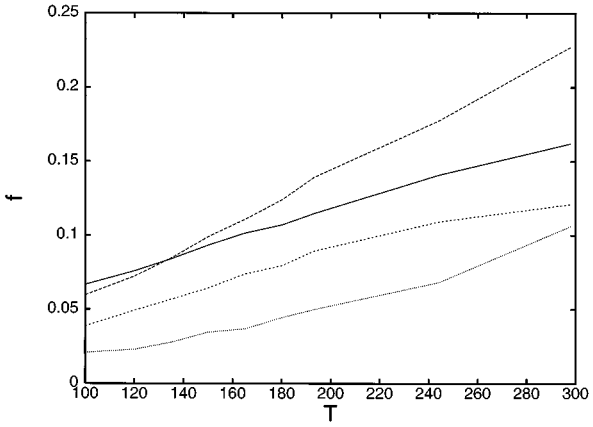

FIG. 8. T dependence of the fractions f_{Im} (solid), $f_{\mathrm{Im}}^{\mathrm{tr}}$ (large dash), $f_{\mathrm{DW}}^{\mathrm{tr}}$ (dotted), and $f_{\mathrm{SH}}^{\mathrm{tr}}$ (small dash).

parent nonzero value of $\langle \rho_{\mathrm{SH}}(\omega=0)\rangle$ is an artifact of finite bin size. Minimal further discussion will be given of SH modes insofar as they, unlike SW and DW, do not yet have clear physical interpretations.

Temperature dependent tr DW dos (Fig. 6) resemble the unprojected DW dos, except the spike is stronger, and the broad background is smaller, as it should be with rotation projected out. It will be shown in the next section that the tr DW modes have a stronger T dependence than do the tr SH or all the tr Im ω modes. The background persisting at low T corresponds, we believe,[19] to the aforementioned rotational influence on the projected tr spectra. The rot DW dos, Fig. 7 has relatively weak T dependence, with the low-ω spike reduced to a low-amplitude shoulder. At high ω and high T, the rot DW dos appear to be reaching a T-independent shape resembling the wings of the tr DW dos, in agreement with the idea that, even in the tr densities, the wing is basically rotational.

III. DIFFUSION

We have given[3,7,12,13] several theories, of varying complexity, for diffusion. In our initial two-flavor study[7] of CS_2, the formula,

$$D = c\langle \omega_i^{\mathrm{tr}}\rangle \Delta f_i^{\mathrm{tr}} \tag{1}$$

was seen to work very well, where c is a constant and i denotes the type of mode chosen to approximate the barriers. In Ref. 7 $i=\mathrm{Im}$, $\langle \omega_{\mathrm{Im}}^{\mathrm{tr}}\rangle$ is the averaged tr Im ω frequency, and the Im ω tr modes remaining at T_g are removed via $\Delta f_{\mathrm{Im}}^{\mathrm{tr}}(T) = f_{\mathrm{Im}}^{\mathrm{tr}}(T) - f_{\mathrm{Im}}^{\mathrm{tr}}(T_g)$; $f_{\mathrm{Im}}^{\mathrm{tr}}(T_g)$ is an estimate of the fraction of false-barrier tr Im ω modes. These modes are primarily the broad background that persists in the tr dos (Fig. 6) at 100 K. If the DW modes are a better approximation to the barrier-crossing modes than are all the Im ω modes, then the choice $i=\mathrm{DW}$ should lead to a smaller subtraction.

Mode fractions f_{Im}, $f_{\mathrm{Im}}^{\mathrm{tr}}$, $f_{\mathrm{DW}}^{\mathrm{tr}}$, and $f_{\mathrm{SH}}^{\mathrm{tr}}$ vs T are shown in Fig. 8; tr fractions are out of all tr modes, while f_{Im} is a fraction of all intermolecular modes. The total Im ω fraction, f_{Im} has a weak T dependence both because of the rotations and the SH. The tr DW fraction $f_{\mathrm{DW}}^{\mathrm{tr}}$ has a stronger T dependence than does $f_{\mathrm{SH}}^{\mathrm{tr}}$ or $f_{\mathrm{Im}}^{\mathrm{tr}}$, and has the smallest remnant at T_g, confirming our expectation. The different T dependences can be seen more clearly in Fig. 9, where the fractions are given relative to their value at $T=298$ K. Not only

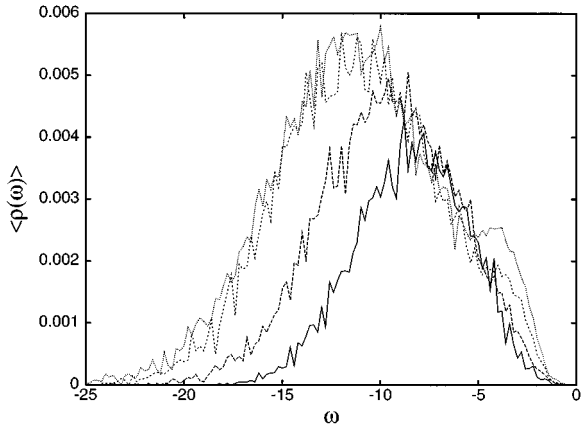

FIG. 7. As Fig. 4 for rotational DW.

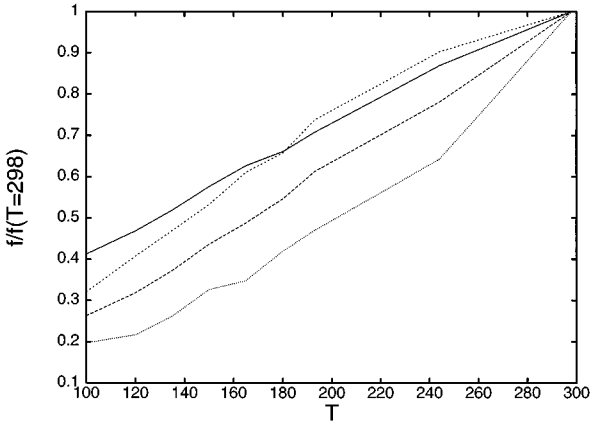

FIG. 9. T dependence of the fractions f_{Im} (solid), $f_{\mathrm{Im}}^{\mathrm{tr}}$ (large dash), $f_{\mathrm{DW}}^{\mathrm{tr}}$ (dotted), and $f_{\mathrm{SH}}^{\mathrm{tr}}$ (small dash), relative to their values at $T=298$ K.

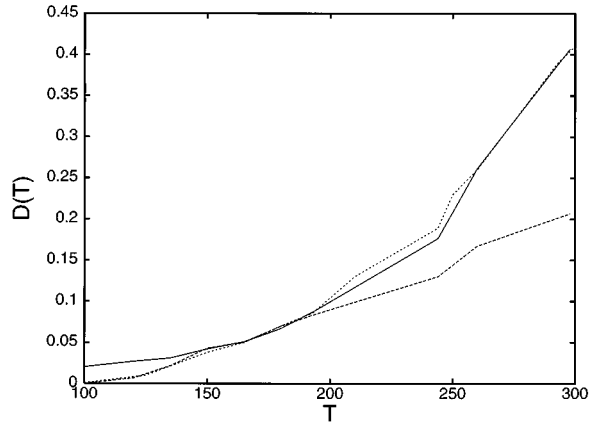

FIG. 10. Comparison of simulated $D(T)$ (small dash) in CS_2 with predictions of Eqs. (1) (large dash) and (2) (solid).

does $f_{\mathrm{DW}}^{\mathrm{tr}}(T)$ have the strongest variation, it has the most curvature, resembling that of $D(T)$. Comparison of Eq. (1) with $i=\mathrm{DW}$ and simulated[7,25] $D(T)$ is in Fig. 10; the value of the adjustable parameter $c=0.50\ \text{Å}^2$, compared to $c=0.17\ \text{Å}^2$ determined[7] previously, because $f_{\mathrm{DW}}<f_{\mathrm{Im}}$. Both the current theory and Ref. 7 exhibit nearly perfect agreement with simulated D throughout the supercooled range and up to 190 and 180 K, respectively. At higher T, deviations set in, with the theory based upon DW showing the better performance.

For CS_2 (Fig. 8), $f_{\mathrm{DW}}^{\mathrm{tr}}\sim f_{\mathrm{SH}}^{\mathrm{tr}}$, and it is also true that $f_{\mathrm{DW}}\sim f_{\mathrm{SH}}$. Bembenek and Laird found[14] $f_{\mathrm{DW}}\gg f_{\mathrm{SH}}$ in LJ, while[9] $f_{\mathrm{DW}}\ll f_{\mathrm{SH}}$ in water. LJ is a fragile liquid and water is strong, with CS_2 somewhere in between; the ratio $\mathrm{S2}=f_{\mathrm{SH}}/f_{\mathrm{DW}}$ follows the strength of the liquid. Thus we propose INM-based probes of strength and fragility. In Sokolov's picture[26] of supercooled liquids, the excitations responsible for intermediate-time dynamics are ''quasilocal harmonic oscillations'' and ''two level systems of a relaxational character.'' In INM, these excitations obviously correspond to SW and DW. Sokolov suggests[26] that strong liquids have a relatively large fraction of harmonic modes, in which case a measure of strength should be $\mathrm{S1}=f_{\mathrm{SW}}/f_{\mathrm{DW}}$. In a supercooled liquid with f_{SW} close to unity and f_{DW} small and strongly T dependent, it is plausible that both S1 and S2 measure strength. A related ratio, that of the number of Re ω to Im ω modes, is denoted (Re/Im).

The ratios depend on T, so one reasonable point of comparison is the melting temperature. Table I compares $\mathrm{S1}(T_m)$, $\mathrm{S2}(T_m)$, and $(\mathrm{Re/Im})(T_m)$ for LJ at reduced density of 0.85, and for CS_2 and water at $P=1$ atm. We have applied our methods to LJ for this comparison, and the water data were obtained as indicated in Ref. 9. The link between S1 and S2 and strength is confirmed. Variation of (Re/Im) is much less than for S1 and S2, because $(\mathrm{Re/Im})=\mathrm{S1}/(1+\mathrm{S2})$, and for large S1 and S2, their increase with strength cancels in (Re/Im). A three-flavor description is essential for construction of the most sensitive probes of strength/fragility, although the trends can still be seen in (Re/Im). The small fraction of Im ω in water was noted by[6] Cho *et al.*, and[8] Ladanyi and Stratt pointed out that the fraction was smaller in polar (stronger) acetonitrile than in nonpolar CO_2.

TABLE I. Strength indicators for fragile (LJ), intermediate (CS_2), and strong (H_2O) liquids.

	LJ ($\rho=0.85$)	CS_2 ($P=1$ atm)	H_2O ($P=1$ atm)
(Re/Im)	4.2	4.5	9.4
S1≡(SW/DW)	5.3	8.4	30
S2≡(SH/DW)	0.26	0.88	2.2

The dimensions of D are l^2t^{-1}; what are the INM DW quantities, for a mode with frequency ω, with these dimensions? Clearly, ω fills the bill for t^{-1}. An INM l^2 is accessible via $U(q)$. Just as an ordinary harmonic oscillator or SW mode has a characteristic mean-square distance from the bottom of the well, $m^{-1}\langle q_\omega^2\rangle_{\mathrm{SW}}$ (q is mass weighted and m is the effective mass), a DW has a mean-square distance from the barrier top, $m^{-1}\langle q_\omega^2\rangle_{\mathrm{DW}}$. Evaluation of $\langle q_\omega^2\rangle_{\mathrm{DW}}$ from $U(q)$ is straightforward. We have for every DW mode the position of the barrier top and the position of the system, that is, q. Dimensional analysis then suggests that we try the formula,

$$D=c'\int d\omega\langle\rho_{\mathrm{DW}}^{\mathrm{tr}}(\omega)\rangle\omega\langle q_\omega^2\rangle_{\mathrm{DW}}, \tag{2}$$

where for simplicity we just let c' be a constant and do not treat ω-dependent effective masses. Equation (2) is compared with simulated D in Fig. 10, with remarkable agreement up to the highest $T=298$ K; $c'=0.25\,\mu^{-1}$. For normal and higher-temperature supercooled liquids, Eq. (2) is quantitatively accurate. At the lowest T, where Eq. (2) predicts too much diffusion, further removal of false-barrier modes could easily be included. The strong T dependence of Eq. (2) compared to that of the different mode fractions demonstrates that INM theories of D depend on more than the number of barrier-crossing modes. The contribution of each mode to D is a nontrivial quantity. In Eq. (2), $\langle q_\omega^2\rangle_{\mathrm{DW}}$, not f_{DW}, dominates the T dependence.

IV. HARMONIC AND ANHARMONIC PROPERTIES OF LIQUIDS

The $U(q)$ contain a large amount of information about liquids. An important caveat is that the INM eigenfunctions change as the particles move, while the $U(q)$ are calculated with eigenfunctions from the initial configuration. In future work, we will[3,11] follow the changing eigenfunctions, but much can be learned about the landscape with the current version. A ubiquitous quantity in INM theories is the frequency dependent mean squared normal coordinate fluctuation, $\langle q_\omega^2\rangle$, which in a classical, harmonic, Re ω system has the value T/ω^2. We can calculate the true $\langle q_\omega^2\rangle_{\mathrm{SW}}$, SW being the mode type most resembling a harmonic oscillator, with the method just applied to $\langle q_\omega^2\rangle_{\mathrm{DW}}$. Comparison with the harmonic expression at 165 K for $\omega\geqslant 3\ \mathrm{ps}^{-1}$ and for $5\ \mathrm{ps}^{-1}\geqslant\omega\geqslant 1\ \mathrm{ps}^{-1}$ is in Figs. 11 and 12. The value of

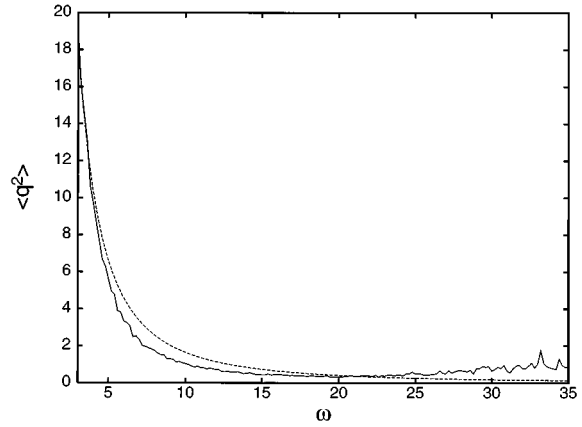

FIG. 11. Simulated $\langle q_\omega^2\rangle_{\rm SW}$ (solid) and harmonic prediction T/ω^2 vs ω (ps^{-1}) at 165 K.

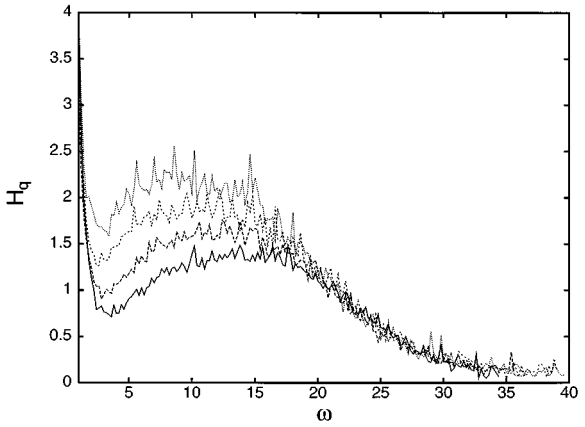

FIG. 13. Harmonicity indicator $H_q \equiv [T/(\omega^2\langle q_\omega^2\rangle_{\rm SW})]$, vs ω at 100 (solid), 165 (large dash), 244 (small dash), and 298 K (dotted).

$\langle q_\omega^2\rangle_{\rm SW}$ falls below the harmonic formula at the lowest ω, is in good agreement at intermediate ω, and exceeds the harmonic formula at large ω. The same general behavior holds for all T, although $\langle q_\omega^2\rangle_{\rm SW}$ does not increase as strongly as $\sim T$ at intermediate ω and the agreement deteriorates with increasing T.

A natural ''harmonicity indicator'' is $H_q \equiv T/(\omega^2\langle q_\omega^2\rangle_{\rm SW})$, shown for four T in Fig. 13. Three frequency ranges are clearly distinguishable, $\omega<2.5\ \mathrm{ps}^{-1}$, $20\ \mathrm{ps}^{-1}>\omega>2.5\ \mathrm{ps}^{-1}$, and $\omega>20\ \mathrm{ps}^{-1}$. For $20\ \mathrm{ps}^{-1}>\omega>2.5\ \mathrm{ps}^{-1}$, which includes almost all the SW modes, the liquid is approximately harmonic, with $2>H_q>0.8$ for all T. Below $2.5\ \mathrm{ps}^{-1}$, H_q rises sharply, signaling an overestimate of $\langle q_\omega^2\rangle_{\rm SW}$ by the harmonic approximation. The explanation is that in a harmonic oscillator q can extend without limit as $\omega\to 0$, while in the liquid a large q will lead to the anharmonic region away from the well bottom, the mode will no longer appear to be a SW, and will not contribute to $\langle q_\omega^2\rangle_{\rm SW}$. Thus we are in accord with Ref. 9 regarding a strong low-ω anharmonicity, except that we would say CS_2 is anharmonic for $\omega<2.5\ \mathrm{ps}^{-1}$, while water is anharmonic for $\omega<7\ \mathrm{ps}^{-1}$.

Anharmonicity increases with T in the intermediate ω regime due to the weak increase of $\langle q_\omega^2\rangle_{\rm SW}$ just mentioned. The idea that only the lower part of the true potential yields a SW is useful here also. As T increases, the new parts of the landscape visited are less likely to yield SW, and $\langle q_\omega^2\rangle_{\rm SW}$ is almost T independent at high T. At $\omega>20\ \mathrm{ps}^{-1}$, $\langle q_\omega^2\rangle_{\rm SW}$ is systematically underestimated by the harmonic formula ($H<1$). A possible explanation can be found in the noticeably anharmonic and asymmetric $U(q)$ prevalent at high ω. The potential in Fig. 14 will yield high ω for negative q, but is very soft, with $\langle q_\omega^2\rangle_{\rm SW}$ enhanced, for positive q. These $U(q)$ resemble the LJ potential, in accord with the idea[27] that the high-ω modes consist of strongly interacting atomic pairs.

The indicator[9] $H_\omega \equiv \langle(\omega_{\rm min}/\omega_{\rm inm})^2\rangle$ is shown in Fig. 15. Encouragingly, the general behavior is the same as that of H_q, with the same three frequency ranges. The low-ω rise, corresponding to a softening of $\omega_{\rm inm}$, and the absence of T dependence in the intermediate-ω range agree with what is observed[9] for water. On the other hand, H_q is T dependent at intermediate ω in CS_2, and[9] no high-ω anharmonicity is found in water. The presence of LJ-like $U(q)$ at high ω can also explain why H_ω is less than unity. For the $U(q)$ in Fig.

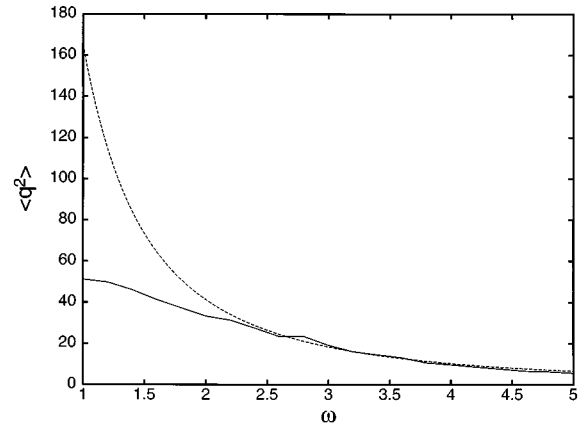

FIG. 12. Low-ω region of Fig. 11.

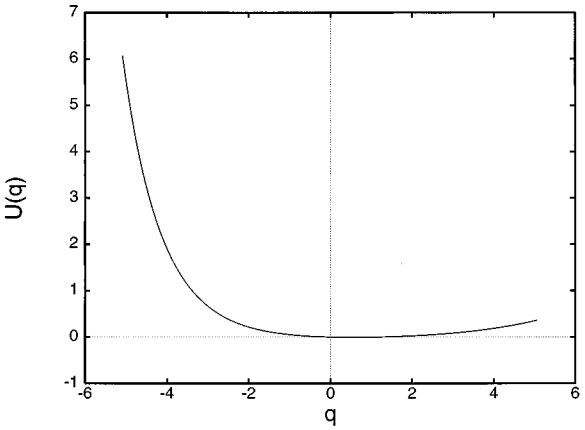

FIG. 14. $U(q)$ for a high-ω SW mode, demonstrating similarity to Lennard–Jones potential; units as Fig. 1.

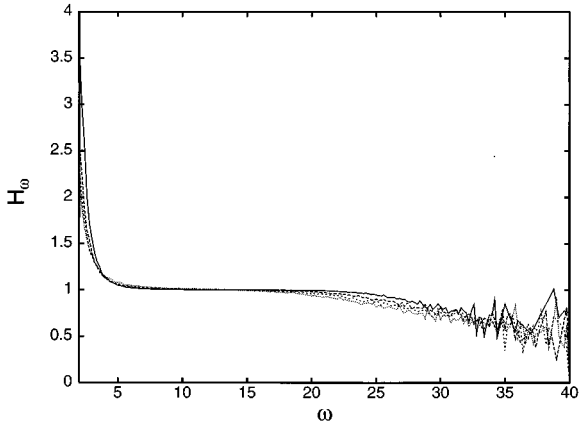

FIG. 15. As Fig. 13 for harmonicity indicator $H_\omega \equiv (\omega_{\min}/\omega_{\mathrm{INM}})^2$, SW modes.

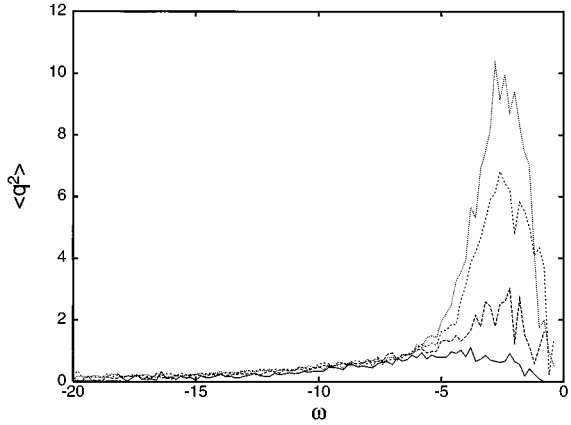

FIG. 16. Simulated mean-square deviation from barrier top for DW modes, $\langle q_\omega^2 \rangle_{\mathrm{DW}}$, in $\text{Å}^2\mu$, vs ω at 100 (solid), 165 (large dash), 244 (small dash), and 298 K (dotted).

14, $H_\omega \ll 1$ at negative q despite the softening at positive q that increases $\langle q_\omega^2 \rangle_{\mathrm{SW}}$. Different indicators and different substances need not display identical behavior; the similarities are more striking than the differences. We are only just beginning, via INM, to pose and answer the question ''how harmonic is a liquid?.''

The low-ω behavior of $\langle q_\omega^2 \rangle_{\mathrm{SW}}$ is significant for future INM development. Integrals arise in some INM theories where[2,3] the integrand is the product of $\langle \rho_s(\omega) \rangle$ and $\langle q_\omega^2 \rangle$; the linear low-$\omega$ behavior of $\langle \rho_s(\omega) \rangle$ and use of the harmonic $\langle q_\omega^2 \rangle = T/\omega^2$ lead to a divergent integrand at low ω. It appears that use of the SW dos with the nondivergent $\langle q_\omega^2 \rangle_{\mathrm{SW}}$ will remedy this difficulty. All modifications of the harmonic formula will affect the time dependence of correlation functions calculated via INM.

Turning to the DW modes, the quantity $\langle q_\omega^2 \rangle_{\mathrm{DW}}$ has already been introduced with Eq. (2). While there exists a harmonic approximation to start with for SW, almost nothing is known about $\langle q_\omega^2 \rangle_{\mathrm{DW}}$, although brief discussions have been given by Cho *et al.*[6] and by Bembenek and Laird.[14] Of course, if the system were literally harmonic with negative curvature, $\langle q_\omega^2 \rangle_{\mathrm{DW}}$ would be divergent. In our case, we simply ask what is $\langle q_\omega^2 \rangle$ given that the mode profile is a DW. If q gets large, the potential changes—the true system is not harmonic—and it is no longer a DW. Results for $\langle q_\omega^2 \rangle_{\mathrm{DW}}$ at several T are in Fig. 16. At high ω, the curves are nearly T independent and are well fit by $\langle q_\omega^2 \rangle_{\mathrm{DW}} \sim 40/|\omega|^2$, strong growth with T sets in for $T > 165$ K and $|\omega| < 6\ \mathrm{ps}^{-1}$, and $\langle q_\omega^2 \rangle_{\mathrm{DW}}$ falls off for the lowest $|\omega|$ due to the cutoff ω_c. The latter two effects combine to generate a peak at $|\omega| \sim 2.8\ \mathrm{ps}^{-1}$, close to the DW translational spike at $3.2\ \mathrm{ps}^{-1}$. Thus for $T \geqslant T_m$, as fluidity increases in the normal liquid, the low-ω tr DW modes grow strongly both in number and in displacement from the barrier top. The T independence at high ω is most likely, again, a signature of rotations. The DW q fluctuations are always much less than those for SW at the same ω, which might support neglect of Im ω modes in theories of time correlation functions.

The harmonicity indicator H_ω may be generalized by the definition $H_\omega \equiv \langle (\omega_{\mathrm{ext}}/\omega_{\mathrm{inm}})^2 \rangle$, where ext denotes the relevant extremum, which need not be the minimum. For DW that extremum is the barrier top and $H_\omega = \langle (\omega_{\mathrm{top}}/\omega_{\mathrm{inm}})^2 \rangle$, showing in Fig. 17 a T-independent decrease from $H_\omega \sim 1$ at high $|\omega|$ to $H_\omega \sim 0.8$ as $\omega \to 0$. While the SW modes soften, evidently the DW ''harden'' as $\omega \to 0$. Nonetheless, the INM frequency is an excellent indicator of the frequency at the barrier top for all ω. This supports the use of INM to calculate barrier crossing rates, since theories require the frequency at the top.

Barrier heights (measured from the lower minimum) are easily read off from DW $U(q)$. The distribution of DW barrier heights, $g(E,T)$, a crucial quantity for diffusion in liquids, is displayed at four T in Fig. 18. It is our sampling that makes $g(E,T)$ depend on T. We only see the barriers which the system visits, i.e., the distribution has the Boltzmann factor folded in and is not a pure landscape property. Barriers with $E \gg T$ are missed in, while those with $E \ll T$ should be well described. The distributions are normalized so there is an apparent change at low E as $g(E,T)$ extends to higher E with increasing T. Notable is the vanishing of $g(E,T)$ as $E \to 0$. This is a consequence of the cutoff ω_c; with no DW modes below ω_c, and with E and ω correlated, the low-E

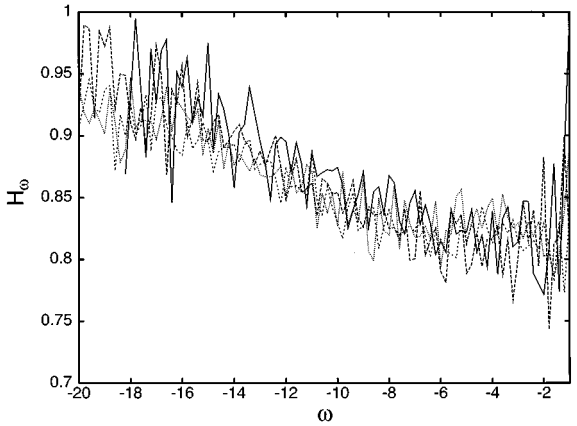

FIG. 17. As Fig. 15 for DW modes, $H_\omega \equiv (\omega_{\mathrm{top}}/\omega_{\mathrm{INM}})^2$.

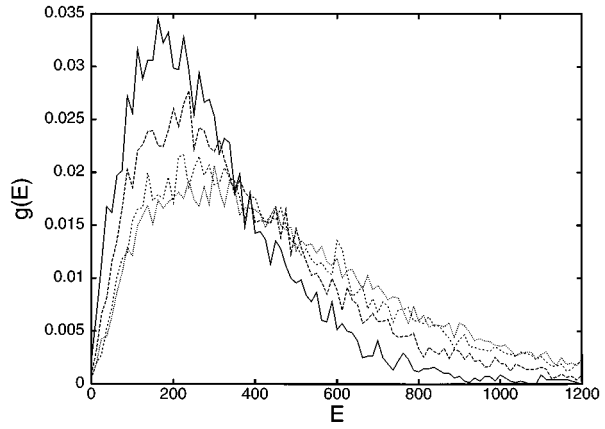

FIG. 18. Distribution of DW barriers, $g(E)$, vs E at 100 (solid), 165 (large dash), 244 (small dash), and 298 K (dotted); E in K.

barriers are depleted. Prior two-flavor studies[12] of $g(E)$ based upon $\langle \rho_u(\omega) \rangle$, with no cutoff, yield a maximum at $E=0$. In our view, the scarcity of low-E barriers causes[12,13] exponential T dependence of $D(T)$.

The relation between E and ω is illustrated in Fig. 19 via the averaged ω-dependent DW energy, $\langle E(\omega) \rangle_{\mathrm{DW}}$, at several T. The increase of $\langle E(\omega) \rangle_{\mathrm{DW}}$ with ω has the elementary interpretation that higher barriers have larger curvature at the top.[12,13] In a now familiar pattern, T dependence is weak at high ω, while a peak at $\omega \sim 3.6\ \mathrm{ps}^{-1}$ grows in for $T > T_m$; the high-ω functional form, governed by rotation, is $\langle E(\omega) \rangle_{\mathrm{DW}} \sim \omega$.

The peak position is close to that ($\sim 3.2\ \mathrm{ps}^{-1}$) in the tr DW dos and it makes sense that the growth in tr DW modes is associated with visiting of higher energy barriers. The data support the idea of an ω-dependent minimum barrier energy. For $T \ll E_{\min}(\omega)$, $E_{\min}$ will dominate the average and $\langle E \rangle \sim E_{\min}$. For $T > E_{\min}(\omega)$, an increase in T will allow the system access to higher barriers and $\langle E \rangle$ can grow with T. As an elementary demonstration of these arguments, note that a horizontal line on Fig. 19 at $T = 298$ K, our highest T, strikes all the data at $\omega \sim 6\ \mathrm{ps}^{-1}$, the boundary between strong and weak T dependence. One might ask why the peak does not begin at lower T and lower ω, where $E_{\min}(\omega)$ is lower. The answer, most likely, is that there are simply not enough modes available as $\omega \to 0$.

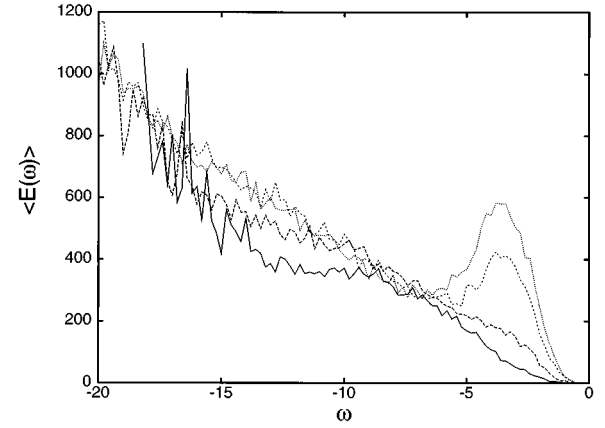

FIG. 19. Average barrier energy for DW modes, $\langle E(\omega) \rangle$, vs ω at 100 (solid), 165 (large dash), 244 (small dash), and 298 K (dotted); E in K, ω in ps^{-1}.

V. DISCUSSION

Analysis of $U(q)$ naturally leads to a three-flavor INM description of liquids. SW modes take the role of local, finite-lifetime harmonic oscillations, replacing the Re ω modes from prior versions. DW modes replace the Im ω modes as barrier-crossing ''relaxational'' excitations.[26] The physical significance of the SH modes remains to be discovered.

This article is a first step. We have presented the three flavor dos and discussed diffusion, strength/fragility, the harmonicity of liquids, the fluctuations of the INM q, and the energy barriers to diffusion. An INM-based assessment of the harmonicity of CS_2 as a function of frequency demonstrates an intermediate-ω harmonic range of $20\ \mathrm{ps}^{-1} > \omega > 2.5\ \mathrm{ps}^{-1}$, with harmonicity at high and low ω.

Several of the results combine to firm up the INM picture of diffusion. Diffusion in normal and supercooled liquid CS_2 has previously[7] been connected with a strongly T-dependent translational peak at Im $\omega \sim 3.2\ \mathrm{ps}^{-1}$, which we now see in the DW dos. In addition, we find almost identical peaks in $\langle q_\omega^2 \rangle_{\mathrm{DW}}$ ($2.8\ \mathrm{ps}^{-1}$) and $\langle E(\omega) \rangle$ ($3.6\ \mathrm{ps}^{-1}$). We may therefore say that diffusion in CS_2 is governed by barriers with $\omega \sim 3\ \mathrm{ps}^{-1}$. At each ω, there is a minimum barrier energy, and $E_{\min}(3\ \mathrm{ps}^{-1})$ is the lowest minimum energy for which there are also an appreciable concentration of barriers. As T is increased sufficiently above $E_{\min}(3\ \mathrm{ps}^{-1})$, which is approximately equal to T_g, higher energy barriers with the same ω are crossed, $\langle E(\omega \sim 3\ \mathrm{ps}^{-1}) \rangle$ increases, and so too does $\langle q^2(\omega \sim 3\ \mathrm{ps}^{-1}) \rangle_{\mathrm{DW}}$. The increase is slow initially and becomes obvious for $T > T_m$. Thus INM illuminates the connection between diffusion and the potential energy landscape in unprecedented detail.

ACKNOWLEDGMENT

This research was supported by NSF Grant No. CHE-9415216.

[1] G. Seeley and T. Keyes, J. Chem. Phys. **91**, 5581 (1989).
[2] R. M. Stratt, Acc. Chem. Res. **28**, 201 (1995).
[3] T. Keyes, J. Phys. Chem. A **101**, 2921 (1997).
[4] F. Stillinger, J. Chem. Phys. **88**, 7818 (1988); Science **267**, 1935 (1995).
[5] M. Buchner, B. M. Ladanyi, and R. M. Stratt, J. Chem. Phys. **97**, 8522 (1992).
[6] M. Cho, G. R. Fleming, S. Saito, I. Ohmine, and R. M. Stratt, J. Chem. Phys. **100**, 6672 (1994).
[7] P. Moore and T. Keyes, J. Chem. Phys. **100**, 6709 (1994).
[8] B. M. Ladanyi and R. M. Stratt, J. Phys. Chem. **100**, 1266 (1996).
[9] F. Sciortino and P. Tartaglia, Phys. Rev. Lett. **78**, 2385 (1997).
[10] J. Kindt and C. A. Schmuttenmaer, J. Chem. Phys. **106**, 4389 (1997).
[11] P. Moore and B. Space, J. Chem. Phys. (to be published).
[12] T. Keyes, J. Chem. Phys. **101**, 5081 (1994).

[13] T. Keyes, G. Vijayadamodar, and U. Zurcher, J. Chem. Phys. **106**, 4651 (1997).
[14] S. Bembenek and B. Laird, Phys. Rev. Lett. **74**, 936 (1995); J. Chem. Phys. **104**, 5199 (1996).
[15] G. Vijayadamodar and A. Nitzan, J. Chem. Phys. **103**, 2169 (1995).
[16] J. Gezelter, E. Rabai, and B. J. Berne, J. Chem. Phys. **107**, 4618 (1997).
[17] F. Sciortino, P. Gallo, P. Tartaglia, and S. H. Chen, Phys. Rev. E **54**, 6331 (1996); Phys. Rev. Lett. **76**, 2730 (1996).
[18] C. A. Angell, Science **267**, 1924 (1995).
[19] W. Li and T. Keyes, J. Chem. Phys. (in press).
[20] D. J. Tildesley and P. A. Madden, Mol. Phys. **42**, 1137 (1981).
[21] G. Herzberg, *Infrared and Raman Spectra of Polyatomic Molecules* (Van Norstrand, New York, 1946).
[22] M. Tuckerman, B. J. Berne, and G. Martyna, J. Chem. Phys. **97**, 1900 (1992).
[23] W. J. Hoover, A. Ladd, and B. Moran, Phys. Rev. Lett. **48**, 1818 (1982); D. Evans and G. Morris, Comput. Phys. Rep. **1**, 297 (1984).
[24] U. Zurcher, T. Keyes, and B. B. Laird (unpublished).
[25] P. Moore (unpublished data).
[26] A. Sokolov, Science **273**, 1675 (1996).
[27] G. Seeley, Ph.D. thesis, Boston University, 1991; R. Larsen, E. David, G. Goodyear, and R. M. Stratt, J. Chem. Phys. **107**, 524 (1997).